AFRL-IF-RS-TR-2002-18
Final Technical Report
February 2002

TRANSPORT PROPERTIES OF BIOFLUIDS IN MICROMACHINED GEOMETRICS

Brown University

Sponsored by
Defense Advanced Research Projects Agency
DARPA Order No. J406/15

APPROVED FOR PUBLIC RELEASE; DISTRIBUTION UNLIMITED.

AIR FORCE RESEARCH LABORATORY
INFORMATION DIRECTORATE
ROME RESEARCH SITE
ROME, NEW YORK

This report has been reviewed by the Air Force Research Laboratory, Information Directorate, Public Affairs Office (IFOIPA) and is releasable to the National Technical Information Service (NTIS). At NTIS it will be releasable to the general public, including foreign nations.

AFRL-IF-RS-TR-2002-18 has been reviewed and is approved for publication.

APPROVED:

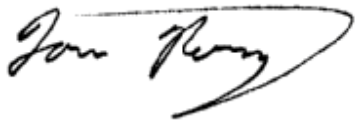

THOMAS E. RENZ
Project Engineer

FOR THE DIRECTOR:

MICHAEL TALBERT, Maj., USAF, Technical Advisor
Information Technology Division
Information Directorate

REPORT DOCUMENTATION PAGE

Form Approved
OMB No. 074-0188

1. AGENCY USE ONLY (Leave blank)	2. REPORT DATE	3. REPORT TYPE AND DATES COVERED
	FEBRUARY 2002	Final Jun 00 – Sep 01

4. TITLE AND SUBTITLE

TRANSPORT PROPERTIES OF BIOFLUIDS IN MICROMACHINED GEOMETRICS

5. FUNDING NUMBERS

C - F30602-00-2-0606
PE - 63739E
PR - E117
TA - 00
WU - 60

6. AUTHOR(S)

Kenneth Breuer

7. PERFORMING ORGANIZATION NAME(S) AND ADDRESS(ES)

Brown University
Office of Research Administration
164 Angell Street, Box 1929
Providence RI 02912

8. PERFORMING ORGANIZATION REPORT NUMBER

N/A

9. SPONSORING / MONITORING AGENCY NAME(S) AND ADDRESS(ES)

Defense Advanced Research Projects Agency
3701 North Fairfax Drive
Arlington Virginia 22203-1714

Air Force Research Laboratory/IFTC
26 Electronic Parkway
Rome New York 13441-4514

10. SPONSORING / MONITORING AGENCY REPORT NUMBER

AFRL-IF-RS-TR-2002-18

11. SUPPLEMENTARY NOTES

Air Force Research Laboratory Project Engineer: Thomas Renz/IFTC/(315) 330-3423

12a. DISTRIBUTION / AVAILABILITY STATEMENT

APPROVED FOR PUBLIC RELEASE; DISTRIBUTION UNLIMITED.

12b. DISTRIBUTION CODE

13. ABSTRACT ***(Maximum 200 Words)***

The determination of transport properties of biological materials flowing in micron and sub-micron geometrics is discussed. The program goal was to develop techniques to identify anomalous viscous and diffusion effects due to complex biological materials. This goal was met. Experimental techniques were developed to accurately measure mass flows and slop velocities present in polymer materials flowing through sub-micron channels. Measurements were taken and preliminary results were obtained indicating that (as expected) polymeric materials do not conform to expected models. More extensive results were not available due to lack of sufficient time during the current program to complete the original investigation.

14. SUBJECT TERMS

Biofluidics, Fluid Transport, Fluidic Channels

15. NUMBER OF PAGES

29

16. PRICE CODE

17. SECURITY CLASSIFICATION OF REPORT	18. SECURITY CLASSIFICATION OF THIS PAGE	19. SECURITY CLASSIFICATION OF ABSTRACT	20. LIMITATION OF ABSTRACT
UNCLASSIFIED	UNCLASSIFIED	UNCLASSIFIED	UL

List of Figures

Acknowledgements

Thanks to the students and Post Docs who have worked on this project – Peter Huang, Zhiqiang Cao, Chang-Hwang Choi and especially to Johan Westin. Also thanks to Chet Klepadlo for his assistance in the lab and to Nancy Congdon for all things financial.

Introduction

The development of advanced microfluidic devices, and biofluidic devices in particular are gated by advancements in many technical fields. These fields include microfabrication, packaging, controls, optical diagnostics, and microfluidic modeling. This last category is often neglected, but in recent years it has been realized that the successful design and operation of efficient, accurate and robust microfluidic devices requires a detailed and sophisticated knowledge of the behavior of fluids in micromachined geometries, and in contact with materials typical of micromachined systems. The goal of this program was to provide (i) a database of fluid properties and (ii) usable models for transport properties of biofluids in conditions relevant to microfluidic systems.

As the microfluidics technology matures, three methods of manipulating fluids at the microscale are emerging as candidates for eventual use in commercial applications. These methods are: conventional pumping, electro-osmotic pumping and pumping by means of acoustic streaming. Each technique has advantages and disadvantages with respect to the pressures that are generated and the flow rates that can be achieved. In addition, the different systems have different effects on fluids and on biofluids in particular. The high-frequency oscillatory nature of some of the pumping schemes (for example those based on "weak valves") can have a detrimental effect on DNA molecules, cell membranes or other structures. Ultrasonic forces are commonly used to rupture cell membranes and might not be desirable for this reason. Lastly, electrokinetic methods of pumping require certain material properties and can also be detrimental to the fluid under study, depending on the particular conditions of the system. Clearly, the mode of fluid/particle/macromolecule transport must be chosen with the both the specific application and the particular biofluid in mind.

It is long recognized that biofluids have unique and complex rheological properties and that the transport processes for non-Newtonian fluids such as blood or fluids with long macromolecules are highly dependent on the geometry and particular strain conditions.

Both the amplitude of the rate of strain, and the frequency at which it varies, have an impact on the viscosity, mass and thermal diffusion of the fluid. In addition, bio-properties, such as adhesion, de-adhesion and clotting as well as metabolic processes are all affected by the fluid strain condition. Lastly, the bio-integrity of the fluid (the survival of DNA strands, cell membranes, etc) is critically dependant on the specifics of the fluid strain profile and these will vary widely depending on the specific geometry and forcing mechanism.
Unfortunately, however, there is a dearth of data regarding such elementary transport properties as momentum and mass transport over the range of conditions found in microdevices, and only anecdotal evidence about the effects on bio-constituents of the strain fields commonly found in microdevices. This lack of data seriously impedes the design and development of advanced micro-biological machines.

Thus, the implementation of micromachined bio-analysis and handling systems introduces a series of questions that need to be answered:
What are the basic transport properties (viscosity, thermal and species diffusion coefficients, etc.) of biofluids in both steady and unsteady flows characteristically found in microscale fluid handling systems
What are the effects of common microscale fluid handling operations on the structure and integrity of bio-materials.

The DARPA/BioFlips program was designed to address these questions through a series of high-precision, carefully controlled experiments designed to generate modeling data for computational design of microfluidic devices. Our approach was to construct a series of increasingly complex test devices each of which measures a transport property in a variety of bio fluids. The test conditions and test devices were designed in such a way as to explicitly test and quantify the properties of the fluids under different forcing conditions, representative of the forcing mechanisms outlined above. Due to the shortened nature of

the program (it ended only one year after it started), only the first of the goals was pursued – that of measurement of viscous effects in micro- and nano-channels.

Previous Work

There are several studies of fluid flow through microchannels of which a few are mentioned here. Gas-flow measurements through micro channels are e.g. reported by Harley *et al.* [2] and Arkilic *et al.*[3],[4]. Accurate mass flow measurements through microchannels with a height of approximately 1.3 μm were undertaken by Arkilic *et al.*, and the results clearly show the presence of slip flow with sub-unity momentum accommodation. It was also shown that the experimental results could be well predicted by a first-order correction for wall slip.

Concerning liquid flow through microchannels, most studies consider slightly larger channel dimensions (typically 10-50μm). However, an early study reporting on experiments in sub-micron scale channels (0.8 μm and 1.7 μm) is Pfahler, Harley and Bau [5]. The working fluid was N-propanol, and surprisingly the results for the two channel heights showed different behavior, with a higher and a lower pressure drop respectively as compared to standard laminar theory without slip effects. They also report on channel plugging when attempting to use de-ionized water.

Studies focused on electrokinetic effects using de-ionized water and saline solutions have been undertaken by Ren, Li and Qu [6]. They used channel dimensions in the range 14-40μm, and they report a quite substantial flow reduction due to electrokinetic forces when aqueous solutions with small ionic concentrations are used. This will be further discussed later.

Finally, in a paper related to the measurements of small volume flow rates, Richter, Woias and Weiss [7], show results with flow rates down to 0.2 nl/s. The basic principle demonstrated in their set-up is to let the flow that passes through the test channel emanate

into a second microchannel with a larger cross section. This second channel is closed with a Pyrex cover to allow optical access. During measurement the channel is partly filled with water to get an observable meniscus. By observing the movement of the meniscus under a microscope the flow rate could be estimated.

Slip effects

The term *slip flow* normally refers to a non-zero velocity at a solid wall, i.e. the commonly used no-slip boundary condition is not valid for the studied flow. This can for instance appear in gas flows where the ratio between the molecular mean free path and the typical geometrical dimensions becomes large. This ratio, which is named the Knudsen number, becomes large if rarefied gases are used and/or the geometrical dimensions are small. Slip flow can also appear in liquid flow containing large molecules (polymers) dissolved in a solvent. In this case the slip flow is not physically a relative motion between the wall and the fluid molecules next to it, but rather an interpretation of the depletion layer that appears near the wall. This near-wall layer is dominated by solvent, giving rise to a local inhomogeneity in the rheological properties which can be interpreted as a slip flow.

The flow of polymer solutions through narrow capillary tubes has been studied experimentally by e.g. Cohen and Metzner [8] (see also Cohen [9]). The tube diameters in their experiment ranged from 190 μm to 1100 μm, and the majority of the data were obtained with aqueous solutions of high-molecular weight polyacrylamide (Separan AP-30) with concentrations from 0.1% to 2%. The results clearly showed abnormally higher flow rates than predicted from viscometric data, and this was interpreted as an apparent slip flow. In order to extend their findings to the narrow channels used in the present study, the data by Cohen and Metzner was first re-analyzed in order to obtain a constitutive relation between shear stress and strain rate for Separan. The analysis is based on Mooney's equation [9], which for tubes with circular cross-section reads

$$\dot{\gamma}_{apparent} = \frac{32Q}{\pi D^3} = \frac{4}{\tau_w^3}\int_0^{\tau_w} \tau^2 f(\tau) d\tau + \frac{8V_s}{D} \tag{1.1}$$

where $\dot{\gamma}_{apparent}$ is the apparent (measured) strain rate, Q is the flow rate, D, the tube diameter, V_S, the slip velocity, τ, τ_w, the shear stress in the bulk and at the wall respectively and finally $f(\tau)$, the constitutive relation for the fluid. For a chosen concentration, the measured (apparent) strain rate and shear stress data from various tube diameters are fitted logarithmically with cubic splines. From these curves, a relation between measured (apparent) strain rate and tube diameter can be extracted for various fixed values of the wall shear stress. Differentiation of Mooney's equation leads to the relation

$$\left.\frac{\partial(32Q/\pi D^3)}{\partial(1/D)}\right|_{\tau_w} = 8V_s \tag{1.2}$$

i.e. a relation between slip velocity and wall shear stress can be obtained from the experimental data. Moreover, extrapolation of the relations between measured (apparent) strain rate and tube diameter provides information about the value of the integral in eq. (1) when the tube diameter approaches infinity. This (virtual) limiting case is useful since it gives a relation between the slip-free strain rate as function of the wall-shear stress. This in turn can be used to extract the constitutive relation *(f(τ))* for Separan. For more details, see Huang and Caswell [11].

Once the constitutive relation is determined, this can be used to estimate the corresponding slip flow effects that can be expected in two-dimensional channels with small gap heights. Mooney's equation for two-dimensional channels is written

$$\dot{\gamma}_{apparent} = \frac{2Q}{h^2} = \frac{1}{\tau_w^2}\int_0^{\tau_w} \tau f(\tau) d\tau + \frac{2V_s}{h} \tag{1.3}$$

where h is the channel height. The results from the predictions are shown in Figure 1, displayed as the ratio between slip velocity and bulk velocity as a function of channel height *(h)*. It is obvious that the slip velocity becomes very large for small channel heights, and thus strongly affects the rheological models that can be used in microchannel flow.

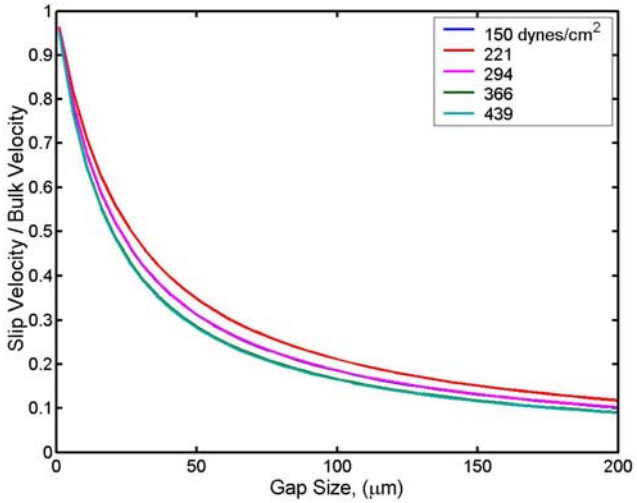

Figure 1. Ratio of slip velocity to bulk velocity as function of channel height for different values of wall-shear stress.

Experimental Methods and Procedures

Microfabrication

The microchannels are made from standard microfabrication techniques, using thermally grown Silicon dioxide to define the channel height. Figure 2 shows a schematic of the more important fabrication steps. Thermal oxide is first grown on a polished silicon wafer using either dry or wet oxidation. The oxide layer is uniform, and gives a good control of the channel height. In the present case the oxide layer thickness is about 1 μm. The second step includes patterning and etching of the channel in the oxide layer. The inlet/outlet ports are etched through the silicon wafer using anisotropic wet etching (KOH, step 3), and finally a second wafer (capping wafer) is bonded to close the channel. The capping wafer for the presently used channels is made of Silicon, but Pyrex wafers can be used instead which

gives the advantage of optical access. The SEM-image in Figure 3 shows the inlet port through the silicon wafer, as well as the channel entrance etched in the silicon dioxide.

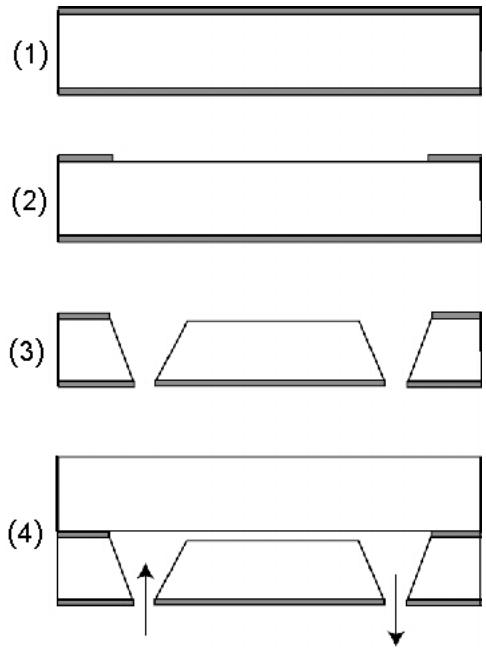

Figure 2. Schematic of microfabrication steps.

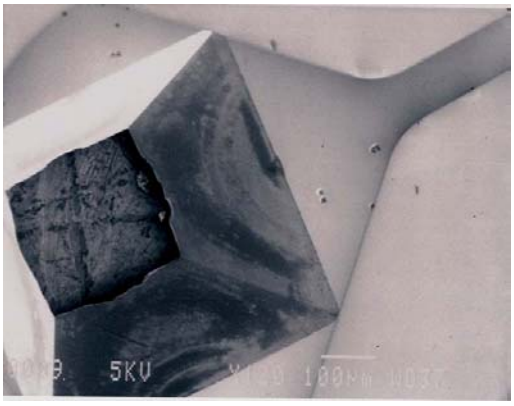

Figure 3. SEM image of inlet port and channel entrance.

Different channel geometries have been used, but most of the results are obtained with the channel shown in Figure 4. The distance between the ports is 10 mm, and the channel has a

spanwise contraction after approximately half the channel length. The channel width varies from 1000 μm to 100 μm, which gives a channel height/width aspect ratio of at least 100.

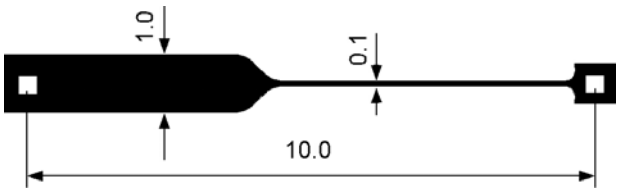

Figure 4. Mask for microchannel. Dimensions in mm.

For deeper channels, thermal oxidation is not possible. In such cases a Silicon on Insulator wafer (SOI) is used which has a precisely defined layer of silicon over a buried oxide layer. By etching the device layer (in a DRIE etcher at the Cornell Microfabrication Facility), a channel is formed which is the bonded to a silicon or glass wafer as described above.

Flow Rate Measurements

The basic principle for the flow rate measurements is to track the movement of the free liquid surface in a precision bore hole using a laser distance meter. Figure 5 shows a schematic of the experimental set-up. The silicon wafer with the microchannel is mounted between two plates made of Stainless steel, and the inlet/outlet ports to the channel are sealed by O-rings. The precision bore hole (ø2 mm) is drilled in the upper plate using electric discharge machining (EDM), and the test sample is loaded into the container with a syringe. The total volume of the container is 17μl, but considerably smaller fluid volumes can be used in a test. The outlet side in Figure 5 is connected to a larger container (ø5 mm), which can be used for test cases requiring higher flow rates. In the present set-up the flow is driven by a pressure difference, using pressurized nitrogen at the inlet side and atmospheric pressure at the channel outlet interfaces. The resolution of the sensor is 0.2 μm, and the specified linearity is within ±0.3% of the full scale range of 2 mm (i.e. ±6μm). In addition to pressure and surface position, the temperature of the Stainless Steel fixture is logged during each test.. Any leakage at the high-pressure side can seriously affect the test results, since the evaporation rate increases if gas is exchanged. For this reason no pressure

regulator is used, but instead the high pressure side is connected to a closed volume (1000cc) with desired pressure. This gives a good control of possible leaks, and the fluid flow rates are small enough to ensure a negligible reduction of the pressure in the system. The surface position is tracked by a laser distance meter (Keyence), which has an active (oscillating) confocal beam that makes it possible to detect transparent gas/liquid

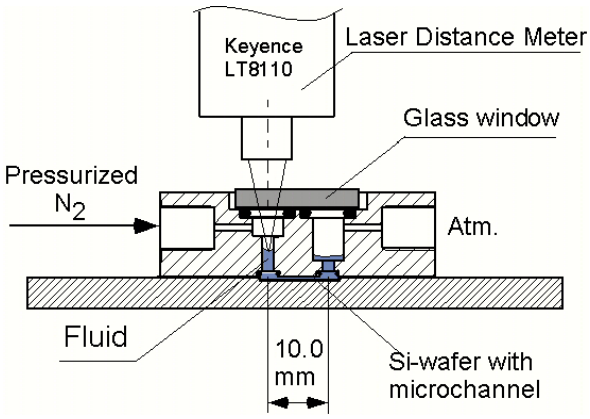

Figure 5. Schematic of experimental set-up.

The entire system is mounted on a servo-controlled three-axis stage. This allows us to keep the laser meter a fixed distance from the minscus height, and to scan several places on the meniscus to determine if the meniscus shape changes as the experiment proceeds.

Measurement Procedures

The surface displacement in a test is typically about 100-500 μm, requiring measurement times of 10-60 min depending on fluid viscosity and applied pressure difference. An example of a test run (ethanol, Δp=0.6 MPa) is shown in Figure 6. The flow rate is determined from a least-square-fit to the entire data set, and the deviation from the curve fit is shown in figure (b). The time variation of the flow rate is monitored by using a local (moving) curve-fit, which in this case is based on a 10 minute average (Figure 6c).

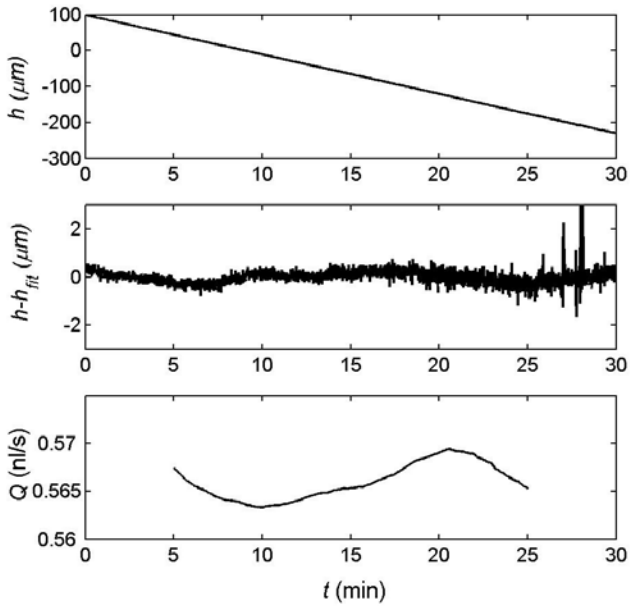

Figure 6. (a) Surface position during a test with Ethanol (Δp=0.6 MPa). (b) Deviation from a linear curve fit to the data. (c) Local flow rate based on a 10 minute average.

Since the measured flow rates are small (less than 1 nl/s) it is important to compensate for evaporation. This is particularly important at low driving pressures and for low-viscosity fluids, which normally have a high vapor pressure. The evaporation rate is estimated by repeating the test procedure without the test channel installed (bottom of the container sealed), and the evaporation rate is consequently subtracted from the measured value.

Results and Discussion

Importance of entrance effects

The pressure drop in the experiments is measured as the total pressure difference between the pressure vessel and the atmosphere. Consequently, this does not only include the pressure drop due to fully developed flow through the channel, but also contributions from the inlet/outlet ports as well as the entrance effect caused by the finite development length needed to obtain fully developed flow. To verify that the additional pressure losses are small and not significantly affect the measured pressure drop, numerical calculations were

carried out. The calculations were made with a finite element code (*Polyflow*), and restricted to two dimensions. The inlet port geometry is shown in Figure 7. The fact that the two-dimensional problem is considered implies that the obtained results should be conservative, i.e. the actual entrance effects for the real three-dimensional case are expected to be smaller.

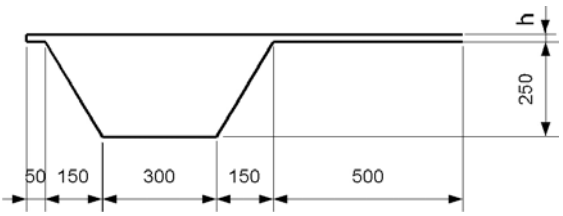

Figure 7. Geometry of inlet port used in 2D-calculation.

One representation of the additional pressure drop due to entrance effects is the "additional length" *(L_a),* which here is defined as the additional (virtual) length that has to be added in order to predict the measured pressure drop by using the assumption of fully developed channel flow. This can be written

$$L_a = \frac{\Delta p_m - GL}{G} \tag{1.4}$$

where $G = dp/dx$, L is the channel length and Δp_m is the pressure drop. .Figure 8 shows the computed values of L_a/L for different channel heights while using water. The channel length is fixed at 10 mm. It is clear that for channel heights less than 100 μm the entrance effects are small (<1%). Calculations were also carried out using a non-Newtonian constitutive model based on a power law assumption, representing a fluid with shear-thinning properties. The results show that the relative entrance effects are larger as compared to those shown in Figure 8, especially for very low Reynolds numbers (small shear). However, even with this model the channel length-to-height ratio has to approach about 100 before these effects become non-negligible. This would correspond to channel heights of about 100 μm for the present case.

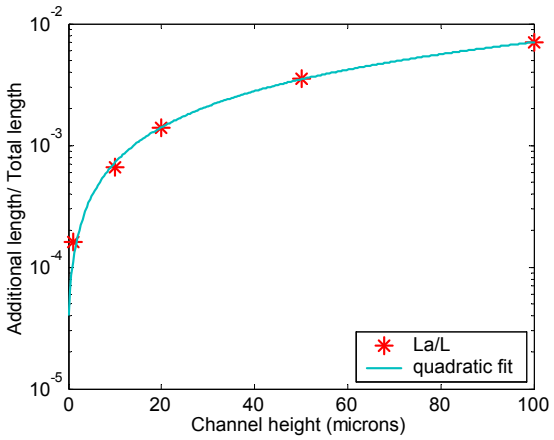

Figure 8. Calculated influence of entrance effects (L_a/L) as function of channel height. Fluid: water.

Deep Channels

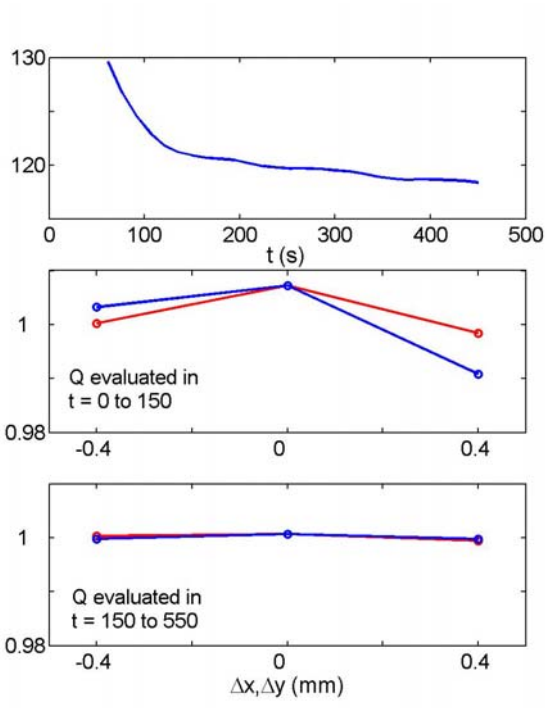

Figure 9. Flow rate (nl/s) as a function of time (top) and relative flow rate (Q) based on five different points on the meniscus and at two different times (middle frame: during the transient; bottom frame: after the transient).

The overall behavior of the experimental system is shown in Figure 9, which plots, in the top frame, the flow rate as a function of time. It is clear that an initial transient exists during which time the flow rate varies quite rapidly, before settling down to a relatively stable value after about 200 seconds. By computing the flow rate based on several meniscus positions, we see that during the transient phase (t = 0 – 150 seconds), the measured flow rate is quite strongly dependent on the location at which the meniscus is monitored, varying by a few percent. However, after the transient has decayed, the position at which the measurement is taken does not affect the result, suggesting that the meniscus has relaxed to a steady state.

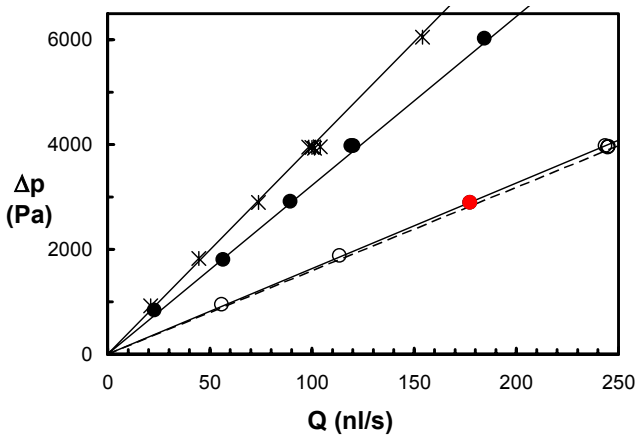

Figure 10. Flow rate in deep channels (19.13 microns). For Silicone oil (open circles), Ethanol (filled circles) and saline solution (stars).

The flow rates in the deep channel (19.12 microns in height) are shown in Figure 10 for three fluids – silicone oil, ethanol and saline solution. The red dot indicates a "calibration point" which is used to adjust the laminar flow constant (which includes all the effects of channel height, width and length). However, the adjustment is very minor (compare the solid with the dotted line), and with this single adjustment, all of the measurements agree very well with the results that are predicted based on bulk viscosity measurements of the fluid (shown as solid lines).

Small Channels

The procedure was repeated for flows in a much smaller channel (870 nm, based on the calibration measurement). The measured pressure drop for different flow rates is shown in Figure 11 for silicon oil (0.65 cSt) and ethanol. Based on the channel height that was determined in the calibration, the pressure drop as function of flow rate can be predicted for Newtonian fluids if laminar Poiseuille flow is assumed and the dynamic viscosity is known. The viscosity is measured by a standard glass viscometer, which gives a measure of the viscosity in a macroscopic environment. The predicted flow rates are included in Figure 11. It should be emphasized that the only experimental inputs to the predictions are the calibration point for the channel height (shown as a bullet in Figure 11) and the macroscopic viscosities measured with the viscometer (which is used to generate the solid lines). The agreement is very good even for flow rates smaller than 0.5 nl/s, which gives confidence that the measurement method can be used for small volume flows. It should also be mentioned that the compensation for evaporation is approximately 4% at the highest flow rates in Figure 11, but more than 40% of the measured value for the smallest flow rates.

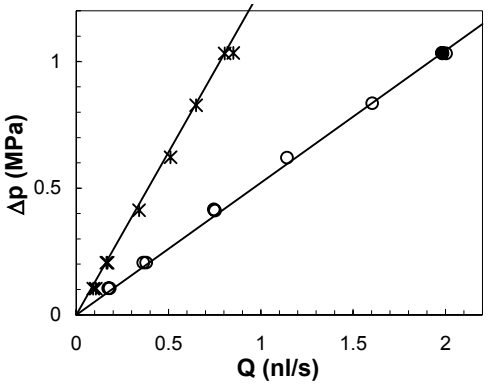

Figure 11. Pressure drop versus flow rate in the 870 nm channel using (o) Silicon oil (0.65 cSt) and (*) Ethanol. Solid bullet shows datum used for calibration of the channel height, and solid lines are predicted flow rates.

Saline solution

One of the primary goals with the present set-up is to test the rheological properties of different biological materials. Since it is common to dissolve biological materials in saline solution, the flow of ionic water through microchannels has to be characterized. However, this has turned out to be more difficult than first anticipated, and not all of the observed anomalies are currently understood. Figure 12 shows the development of the measured flow rate during 3 hours obtained with a 0.1M (moles/liter) solution of sodium chloride in DI-water. Corresponding tests with ethanol is included for comparison. While the results with ethanol show a relatively constant flow rate with time, the saline solution exhibits a clear decrease in flow rate: a rapid decrease during the initial 20-30 minutes, followed by a slower but fairly constant flow rate reduction during the entire measurement. It should also be emphasized that the measured flow rate with saline solution is too small as compared to predictions based on the Poiseuille flow assumption. Considering the viscosity ratio between ethanol and saline obtained from viscometer measurements, the flow rate of Saline through the microchannel should be approximately 1.1 nl/s in Figure 12.

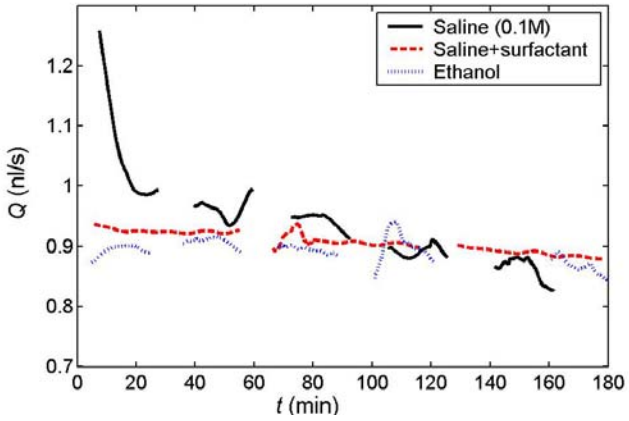

Figure 12. Measured flow rate as function of time. The flow rate is calculated from a local (moving) curve-fit based on 10 minutes of data.

As discussed above, the reason for the first (rapid) transient has been identified to a change in the shape of the free surface. A basic assumption in the present measurement technique is a quasi-stationary shape of the surface, i.e. we assume that the curvature of the meniscus

does not change while the liquid is moving through the cavity. By adding a drop of surfactant (Triton X-100), the initial transient was eliminated (see Figure 12). When the driving pressure suddenly is increased at the beginning of a test the shape of the meniscus will change. Apparently the high surface tension of water is slowing down this reshaping process, and consequently causing an erroneously high estimate of the flow rate. Neither ethanol nor silicon oil, which both are considerably more wetting on stainless steel than water, show no sign of such initial transient.

The continuous slow decrease of the flow rate when using saline is more difficult to explain, and at the present time no definite explanation is available. It can be seen in Figure 12 that the decay rate is smaller when a surfactant is added to the fluid, but the effect is still present. Possible explanations will be discussed later.

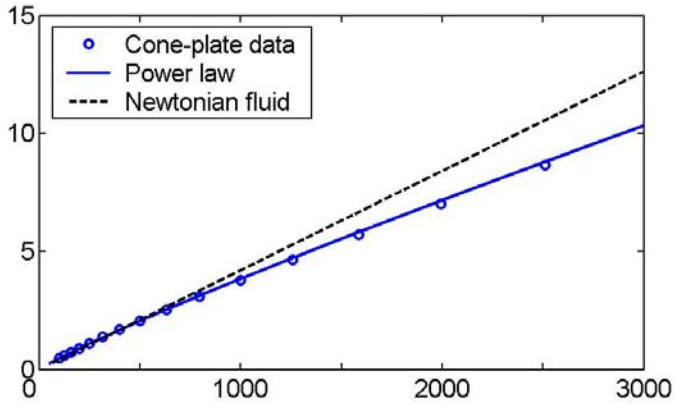

Figure 13. Macroscopic cone-and-plate data for a weakly shear-thinning polymer solution. This fluid has a power law stress-rate of strain relationship with n = 0.9.

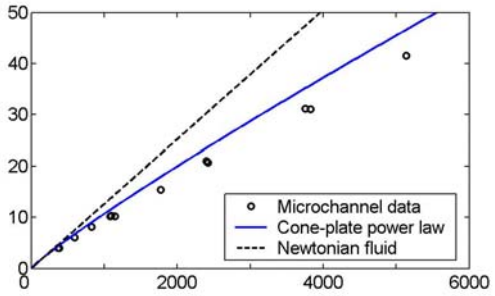

Figure 14. Stress vs, rate of strain for polymer fluid in a 19.13 micron channel. The solid blue line represents the predicted behavior based on the macroscopic cone and plate measurements, the dotted line is the predicted behavior for a Newtonian fluid.

Polymer solutions

Initial tests with a dilute polymer solution have been undertaken (0.25% polyacrylamide, molecular weight 5 million, dissolved in saline). The macroscopic cone and plate data (made in G. McKinley's lab at MIT) are shown in Figure 13, and indicate a weakly shear thinning fluid with a power law exponent of 0.9. However, in the micro channel, the flow rate measured as a function of applied pressure is higher than predicted by this power law (Figure 14), suggesting that a slip velocity is present at the wall in the polymer depletion layer. By applying Moony's equation, discussed earlier, the slip velocity is shown to be about 15% of the bulk velocity (Figure 15), and independent of the shear rate.

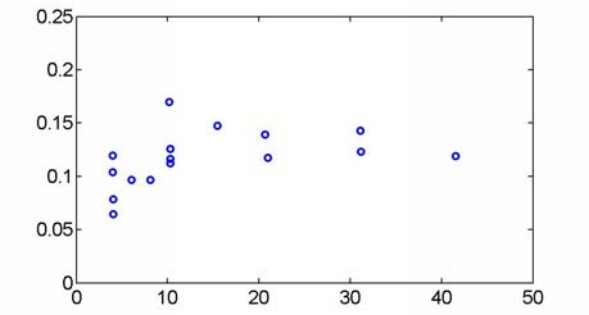

Figure 15. Slip velocity as afunction of wall shear stress for the polyacrylamic solution, obtained using Moony's law.

Discussion of anomalous saline effects

As shown in Figure 12 the flow rate of saline solution slowly decays with time, and the same behavior can also be observed for de-ionized water. One possible explanation could be an increasing presence of dissolved nitrogen in the fluid as the test progresses. Since the gas solubility in a fluid is influenced by pressure, there is a possibility that dissolved nitrogen is released from the fluid when the static pressure decreases along the channel. The nitrogen concentration in the fluid entering the channel is also limited by diffusion. An order of magnitude estimate of the required diffusion time for nitrogen in water shows that about 3-4 hours is needed for diffusion through the initial column height in the cavity. However, long time pre-pressurizing of the test fluid in order to remove possible concentration gradients has not completely removed the decaying trend in the flow rate measurements, so the results are not conclusive in this respect. Another issue is why no such trend can be observed in the case of ethanol, since both the solubility and the diffusion coefficient are higher for nitrogen in ethanol as compared to water. This may be explained by the lower surface tension in ethanol, which could imply that released nitrogen forms smaller bubbles with less influence on the flow through the microchannel. However, as pointed out above, the hypothesis of dissolved nitrogen as the cause of the decaying flow rate is only one possible explanation among others. For instance surface chemistry, with possible time dependent changes of the surface properties, may have an influence on the present results.

Electrokinetic effects

Irregardless of the slow decay in the flow rate as time increases, the other unexplained observation is the low flow rate obtained with water and saline solution. The flow rates shown in Figure 12 are roughly 20% smaller than predictions based on the Poiseuille flow assumption. A possible candidate to account for the increased pressure drop is electro-kinetic effects. Since the silicon walls (covered with a thin lining of silicon dioxide) have a

non-zero surface potential, ions dissolved in the fluid will form a potential gradient normal to the walls. Some counter-ions attach to the wall, and then there is a gradual decrease of counter-ion concentration until the bulk concentration is reached. Together this forms the so-called electric double layer (EDL). If the thickness of the EDL is sufficient, there will be a net transport of counter-ions in the streamwise direction due to the velocity of the fluid. The result is a streamwise potential difference (denoted streaming potential), which will create an opposing electrical force on the ions in the fluid. If the streaming potential effect is significant, the fluid flow is affected resulting in an increased pressure drop for a given flow rate. An important parameter for the strength of the streaming potential is the thickness of the electric double layer, which in turn is determined by the ion concentration. The EDL thickness increases with decreasing ion concentration, which implies that the largest effects of the streaming potential can be expected for de-ionized water (which contains a small but finite ion concentration). Consequently, by adding salt to increase the ion concentration, the EDL-thickness can be made very thin and thus minimizing the opposing force due to the streaming potential.

Electrokinetic flow through fine capillaries has been studied analytically/numerically by Burgreen and Nakache [12], and later both experimentally and numerically by the group of Li (see for instance Ren, Li and Qu [6], Mala *et al.* [13]). Ren *et al.* used a specially designed experimental set-up in order to measure the streaming potential, using channel heights in the range 14-40 μm. In some of their cases they report an increased pressure drop of about 20% in both experiments and calculations.

To check whether electrokinetic effects can play a role in the present experiment, both calculations and experiments with saline solutions of different concentration were carried out. The calculations followed the procedures described by Ren *et al.* [6], but since the present experiment is not designed for direct measurements of the electrokinetic effects some assumptions must be made. Similar to Ren *et al.* the surface conductivity is neglected, and the value of the Zeta-potential, i.e. the wall boundary condition for the

electro-static potential, is set to 0.2 V. This is similar to the values determined by Ren *et al.* for de-ionized water near a silicon surface. Another uncertainty, however, is the fact that the fixture used in the present experiment is conducting (stainless steel), which has not been taken into account in the present estimate. Nevertheless, based on those assumptions the calculations show that for a dilute NaCl-solution ($5 \cdot 10^{-5}$ M) in a 0.87 μm high channel the flow rate can be reduced with approximately 15% at a given pressure drop. However, the calculation results in a streaming potential of about 65 V for the present channel dimensions, which differs significantly from the experimental values of less than 100 mV reported by Ren *et al.* [6] for a 14 μm high channel. (Our own calculations with this channel height show even larger difference). At the present time it is not known whether this discrepancy is due to a mistake in the calculations/ assumptions, or if it is an indication that the real electrokinetic effects are smaller than predicted.

Although the calculated estimate indicates that electrokinetic effects might give an observable flow reduction, the tests with various salt concentrations do not support this hypothesis. By increasing the salt concentration to 0.1M the predicted effect of the streaming potential should become negligible, since the thickness of the EDL reduces to a few nanometers. Our experimental results, however, do not show a clear effect when varying the concentration, and the measured flow rate is still about 15% lower than expected. Consequently, it can not be concluded that electrokinetic effects are influencing the flow in the present experiment, and other possible explanations are now under investigation.

Conclusions

Despite the truncated nature of the program, we consider it to be a technical success and we achieved the primary goals of the program:

An experimental set-up designed for pressure driven liquid flow through microchannels was developed and tested. The primary aim is to study the transport properties of

complex fluids, e.g. to determine shear dependent viscosities and possible slip effects near the walls.
Re-analysis of available experimental data (Cohen & Metzner [[8]]) for dilute polymer solutions showed that the contribution from slip flow should be very large when the channel height is reduced to micron-scale.

Silicon microchannels with a heights ranging between 50 μm to less than 0.9 μm have been fabricated with good precision.

The geometries fabricated have been tested in the experimental set-up, and the results for Newtonian fluids (silicon oil, ethanol) show very good agreement with predictions also at flow rates ranging from 0.2 to 2 nl/s. This implies that the macroscopic description, assuming laminar Poiseuille flow without wall-slip, is still valid for these fluids under these conditions. However, in the small channels when using aqueous solutions (de-ionized water, saline of different concentrations) the experimental results exhibit different anomalies. Several phenomena are thought to be responsible for the discrepancies, but we are currently unable to explore these idea.

Polymer solutions, characteristic of biological materials have been tested and indicate significant slip velocities and non-Newtonian characteristics, even in large channels (h = 19.31 μm). This last point was the expected result at the outset and we have now verified its existence. Unfortunately, we cannot explore it further under the current program.

Recommendations

As expected, we find that there are strong departures from standard descriptive models as complex fluids are used in micron and sub-micron geometries. In order for accurate design of microbiological systems to be a reality, these departures must be understood and characterized. Wall velocity measurements, non-Newtonian effects, etc are present and unless characterized, will lead to poor micro and nano-device design and modeling. The

original program had also targeted electrokinetic flows as well for such study and these still need to be done. The recommendation is thus to continue this effort.

References

[1] Levy, M.S., Collins, I.J., Yim, S.S., Ward, J.M., Titchener-Hooker, N., Ayazi Shamlou, P., Dunnill, P., 1999, "Effect of shear on plasmid DNA in solution", *Bioproc. Eng.,* **20**, 7-13.

[2] Harley, J., Huang, Y., Bau, H., Zemel, J., 1995, "Gas-flow in microchannels", *J. Fluid Mech.*, **284**, 257-274.

[3] Arkilic, E.B., Scmidt, M.A., Breuer, K.S., 1997, "Gaseous slip flow in long microchannels*", J. MicroElectroMechanical Systems*, **6** (2), 167-178.

[4] Arkilic, E.B., Breuer, K.S., Schmidt, M.A., 2001, "Mass flow and tangential momentum accomodation in silicon micromachined channels*", J. Fluid Mech.*, **437**, 29-43.

[5] Pfahler, J., Harley, J., Bau, H., 1990, "Liquid transport in micron and submicron channels", *Sensors and Actuators A21-A23*, 431-434.

[6] Ren, L., Li, D., Qu, W., 2001, "Electro-viscous effects on liquid flow in microchannels", *J. Coll. Interface Sci*., **233**, 12-22.

[7] Richter, M., Woias, P., Weiss, D., 1997, "Microchannels for applications in liquid dosing and flow-rate measurement", *Sensors and Actuators A62*, 480-483.

[8] Cohen, Y., Metzner, A.B., 1985, "Apparent slip flow of polymer solutions", *J. Rheol.*, **29**(1), 67-102.

[9] Cohen, Y., 1981, "The behavior of polymer solutions in non-uniform flows", PhD thesis, Univ. of Delaware, Newark.

[10] Mooney, M. 1931, "Explicit formulas for slip and fluidity", *J. Rheol*. **2** (2), 210-222.

[11] Huang, P. and Caswell, B. "Design of microchannels for the detection of slip flow in polymer solutions". Manuscript in preparation.

[12] Burgeen, D., Nakache, F.R., 1964, "Electrokinetic flow in ultrafine capillary slits", *J. Phys. Chem.* **68**, 1084-1091.

[13] Mala, G.M., Li, D., Werner, C., Jacobasch,H.-J., Ning, Y.B. 1997, "Flow characteristics of water through a microchannel between two parallel plates with electrokinetic effects", *Int. J. Heat and Fluid Flow*, **18**, 489-496.